



# REVIEW OF RESEARCH

ISSN: 2249-894X

IMPACT FACTOR : 5.7631 (UIF)

UGC APPROVED JOURNAL NO. 48514

VOLUME - 8 | ISSUE - 9 | JUNE - 2019



## SYNTHESIS AND CHARACTERIZATION OF COVALENT TRYPTOPHAN SINGLE AMINO ACID DERIVED PEPTIDE NANOTUBES- CAFFEINE CONJUGATES

R. Govindhan<sup>1,2,3</sup>, D. M. Muniraj<sup>2</sup> and B. Karthikeyan<sup>3</sup>

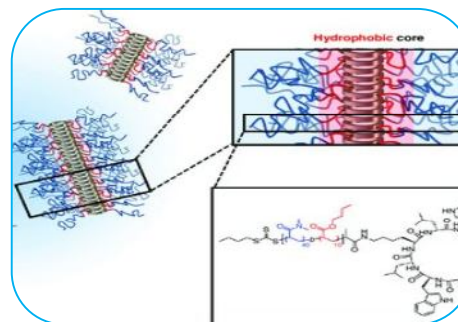
<sup>1</sup>Department of Chemistry, Sri Vijay Vidyalaya college of Arts & Science, Dharmapuri, Tamilnadu, India.

<sup>2</sup>Department of Chemistry, Periyar University Constituent College, pappireddipatti, Tamilnadu, India.

<sup>3</sup>Department of Chemistry, Annamalai University, Annamalainagar 608 002, Tamilnadu, India.

### ABSTRACT

Herein we describe the synthesis and interactions between self-assembled 3,5-bis(trifluoromethyl)benzylamine derived tryptophan (T) amino acid formed peptide nanotubes (BTPNTs) and caffeine conjugates studied through spectral and microscopic tools. The characterization techniques: HR-SEM, HR-TEM, Confocal Raman spectral and microscopic analysis (CRS and CRM), FT-Raman and optical absorption spectroscopy were used to understand the nature bonding of synthesized BTPNTs and caffeine conjugates. The conjugate was obtained via chemical functionalization through coupling of amine group of BTPNTs and carbonyl and methyl groups of caffeine. The surface analysis of BTPNTs-caffeine indicated the presence of caffeine aggregates on the surface of BTPNTs. Identification of possible interactions and surface morphological changes of BTPNTs-Caffeine studied using drug delivery and sensing applications.



**KEY WORDS:** - Tryptophan amino acid; Caffeine; CRS and CRM; BTPNTs; DDS; Sensors.

### INTRODUCTION:

In recent scenario, there has been an increasing interest in the fabrication of new nanoscale material assemblies for diagnostics and treatment of a variety of diseases like Alzheimer's [1-3]. Selective recognition and sensing of transition metal ions attract, increasing studies due to their significant importance in chemical, biological, and environmental processes [4-7].

Peptide nanosystems discovered functional applications in biology and medicinal sciences. A recent research established that the formation of nanotubes (NTs) using self-assembly of dipeptide like Phe-Phe and insertion of metal micro/nanoparticles inside the NTs [8-13]. The peptide nanotubes were stable up to 150 °C and in a wide range of pH [14]. Ancient times few

findings, several approaches have been devised to become stable these nanotubes apart from the interactions like electrostatic,  $\pi$ - $\pi$ , zipper, and stacking etc. [15-21]. Raman spectroscopy has the capability, making 3,5-bis(trifluoromethyl)benzylamine derived T peptide nanotubes (BTPNTs) to be awarding SERS activity and it creates sensitivity. Surprising physicochemical properties of peptide nanotubes

are allowed to enhance the performance, particularly in the field of imaging and targeted drug delivery system (DDS) applications [22–26].

The natural compounds like theoflavin [27], cyclodextrin [28] are capable of binding caffeine through hydrophobic covalent interactions. Caffeine shows heterogeneous association with different carboxylic acids [29–32], hydroxy acid and simple heterogeneous stacks with methyl gallate [33] in their solid state. In recent times some investigations [34,35] reported the interaction of caffeine with polyphenols, which are in attendance in the preparation of black tea, coffee and tea creaming. In aqueous solutions, the interaction of caffeine has also been studied with zinc based porphyrin peptide type receptor [36]. So it would be attractive to study the interface of caffeine with self-assemblies to find out the communication with such systems.

Caffeine is also one of the most generally inspired psycho-stimulant substances. It is mostly obsessive in the form of coffee or tea. It is primarily acting on the central nervous system [37–39]. The role of other components in coffee and the highly complex mechanism of caffeine action are still not completely understood. Caffeine consumption through coffee has been found to be inversely associated with threat of certain types of cancer, type II diabetes, and Parkinson's and Alzheimer's disease [40,41]. Eventhough the improvement of nanotechnology fabrication in prospective to generate novel structures with improved abilities to penetrate through cell membranes, and increased solubilization, stability and produces bioavailability of biomolecules, distribution their delivery efficiency. NTs recommend opportunities for wide range of applications including bio-imaging and targeted delivery of bio-macromolecules into cells [42].

In this work, we unite the outstanding chemical and biological properties of BTTPNTs and caffeine molecules. We early present the covalent synthetic procedure to conjugate self-assembled BTTPNTs and caffeine. Subsequent, the obtained conjugates were characterized by using microscopic tools, and results show confirmation of identical caffeine binding to BTTPNTs. The applicability of BTTPNTs-caffeine assemblies for DDS and bio-imaging related applications was investigated using HR-SEM microscopy. CRS and CRM, Fourier Transform Raman scattering spectroscopy (FT-Raman) is a noninvasive technique that can offer molecular composition, conformation, and vibrational assignments of BTTPNTs [43] is highly suitable for characterizing samples containing trace amounts of target molecules. Finally, we conclude that the synthetic method preserve the molecular structure of caffeine which is essential for covalent binding of BTTPNTs.

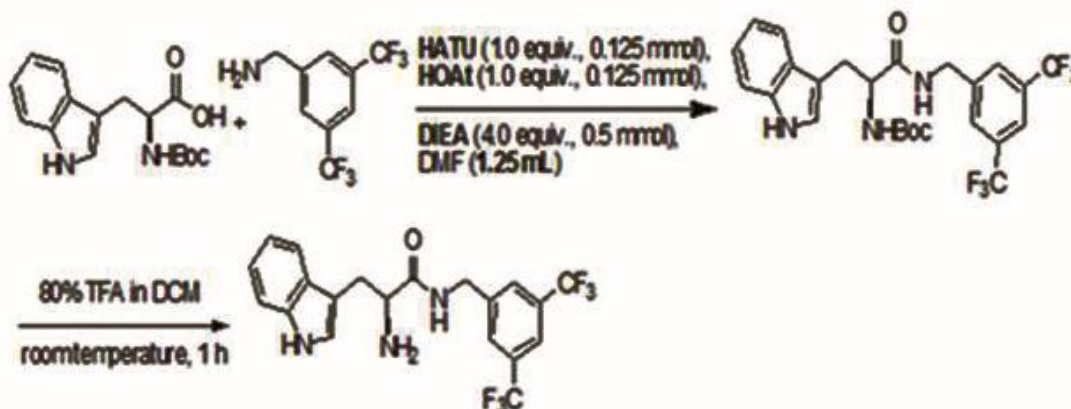
## 2. EXPERIMENTAL SECTION

### 2.1. Materials and methods

3,5-Bis(trifluoromethyl)benzylamine, 98.0%; Boc-AA-OH (AA = Tyr, 1.0 equiv., 0.125 mmol, 42 mg for Tyr); HATU (1.0 equiv., 0.125 mmol, 47.5 mg); HOAc (1.0 equiv., 0.125 mmol, 17 mg) and DIEA (4.0 equiv., 0.500 mmol, 0.087 mL) in dry DMF (1.25 mL) were bought from AAPTEC, USA. KHSO<sub>4</sub>, 99.0%; Caffeine, 99.0%; DCM, 98.0%; TFA, 98.0% solution and other reagents and solvents were purchased from HiMedia Laboratories Pvt. Ltd. (Mumbai, India). All the chemicals were used without further purification. All aqueous solutions were prepared with nanopure water. All apparatus and glassware's are washed with acetone, rinsed with deionized water (DIW) and dried with air hot oven at 100 °C, then it was used throughout the studies.

### 2.1.1. Synthesis of 3,5-bis(trifluoromethyl)benzylamine derivatives of tryptophan peptide (BTT peptide)

3,5-Bis(trifluoromethyl)benzylamine (1.0 equiv., 0.125 mmol, 30.5 mg) was added to a solution of Boc-AA-OH (AA = Try, 1.0 equiv., 0.125 mmol, 42 mg for Tyr), HATU (1.0 equiv., 0.125 mmol, 47.5 mg), HOAc (1.0 equiv., 0.125 mmol, 17 mg) and DIEA (4.0 equiv., 0.500 mmol, 0.087 mL) in dry DMF (1.25 mL) at room temperature. The reaction mixture was stirred for overnight (20 h) and then



quenched with 0.5 M aqueous solution of  $\text{KHSO}_4$  (5 mL). It was then extracted with DCM ( $3 \times 15$  mL). The combined organic part was subsequently washed with brine, saturated sodium bicarbonate and again brine. Evaporation of DCM under reduced pressure using rotary evaporator gave the crude product in quantitative yield. The Boc group was removed by treating the product with 80% TFA in DCM for 1 h at room temperature [38]. Removal of volatiles provided the unprotected bis(trifluoromethyl)benzylamine derivative of the respective single amino acid. Washing with 1:4 solutions of ether and hexane ( $3 \times 10$  mL) provided the final product in >80% yield with <95% (HPLC) shown in Scheme 1.

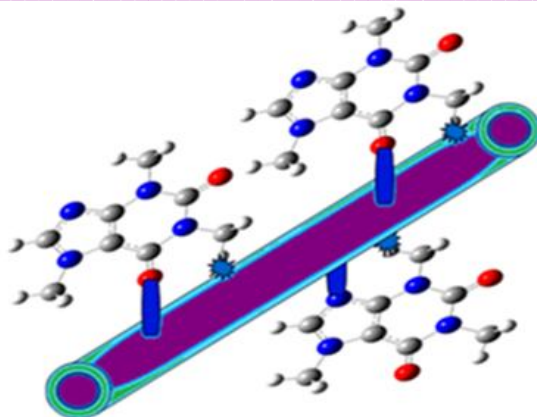
**Scheme 2.1.** Schematic illustration for the solid phase synthesis of 3,5-bis (trifluoromethyl) benzylamine derivative of tryptophan peptide (BTTP).

### 2.1.2. Synthesis of self-assembled BTT peptide nanotubes (BTTPTNTs)

The procedure was adopted from a reported method [38] as follows. About 10 mg of aqueous solution (in nanopure water) of single amino acid derived tryptophan peptide was prepared in a 100 mL beaker with appropriate concentration. The beaker containing desired solution and a magnetic stir bar was sited in pre-warmed silicon oil bath ( $65^\circ\text{C}$ ) and moderate stirring was continued for 30 min at that temperature. Heating was stopped and the solution was brought to room temperature with gentle stirring for over a period of 3 h.

### 2.1.3. Synthesis of caffeine coated on BTTPTNTs (BTTPTNTs-caffeine)

A synthetic procedure for loading the peptide nanotubes was briefly outlined in Scheme 2. Briefly, caffeine solution (5 mL) taken in a beaker and stirred for 30 min at room temperature. As-synthesized BTTPTNTs sol (1 mL) was added slowly into the beaker containing caffeine solution with drop wise manner. The mixture was stirred for another 30 min at room temperature to form BTTPTNTs-caffeine sol, which resulted in the formation of thick sol-gel turbidity containing the BTTPTNTs-caffeine material.



**Scheme 2.2. The covalent interactions of caffeine implanted BTTPNTs (BTTPNTs-caffeine).**

## 2.2. Characterization methods

UV-vis absorbance spectra were recorded over a range of 200–800 nm with a Shimadzu UV-1650PC spectrometer, operated at a resolution of 0.5 nm. The samples were filled in a quartz cuvette of 1 cm light-path length, and the absorption spectra were given in reference to deionized water and distilled ethanol. Confocal Raman spectral and microscopic analysis (CRS and CRM) was recorded using STR micro Raman spectrometer (Model STR 300) with 532 nm 100 mW laser source. The STR micro Raman spectrometer was first calibrated using silicon and naphthalene. Reference spectra were obtained from silicon and naphthalene using 532 nm laser (power 100 mW) with 600 g mm<sup>-1</sup> gratings for 1 s and ×50 objective lens. FT-Raman spectrum was recorded in an integral microscope Bruker RFS 27 spectrometer equipped with 1024×256 pixels liquid nitrogen-cooled germanium detector. A monochromatic beam of incident radiation of wavelength 1064 nm emitted from neodymium doped yttrium aluminium garnet (Nd-YAG) laser was used as an excitation source. High-resolution transmission electron microscopy (HR-TEM) images were recorded using a JEOL 3010 high resolution transmission electron microscopy with an ultra-high resolution (UHR) pole-piece operates at an accelerated voltage of 300 kV. HR-TEM image was enhanced by using image J viewer software. The analyte for HR-TEM studies were prepared by depositing a drop of the synthesized sample on a carbon coated Cu grid and allowing it to evaporate. The high resolution electron microscopy (HR-SEM) was carried out on a FEI Quanta FEG 200 instrument facility at 25 °C. The sample was prepared by placing a small quantity of the prepared material on a carbon coated copper grid and allowing the solvent to evaporate.

## 2.3. Theoretical calculations

Optimization of the ground state geometry and simulation of vibrational spectra of BTTPNTs and covalently interacted BTTPNTs-caffeine were deliberate by a DFT method of Becke, three-parameter, Lee-Yang-Parr (B3LYP)/6-311G\*\*, using the Gaussian 09W software [39]. The B3LYP functional yields reliable results for BTTPNTs in former studies and has been consistent for predicting energy gap values. DOS plots were imitation with Gausssum program wrap up [40].

## 3. RESULTS AND DISCUSSION

### 3.1. UV-vis spectral analysis

**Figure 3.1** shows the UV-vis spectra of caffeine and BTTPNTs-caffeine. **Figure 3.1a** displays the optical absorption peak observed as one at 357 and another at 516 nm. It indicates that  $\pi-\pi^*$  and  $n-\pi^*$  transitions are occur in caffeine molecules. These transitions are renowned in literature [36, 37] and further these two transitions are demonstrated by the HOMO, LUMO diagram which is given in **Fig. 3.8**. **Figure 3.1b** shows the absorption peak intensities of caffeine are abridged and

blue shifted (357 nm) and a new (283 nm) peak is formed. This shift is due to charge transfer from caffeine to BTPPNTs (**inset: Fig. 3.1**).

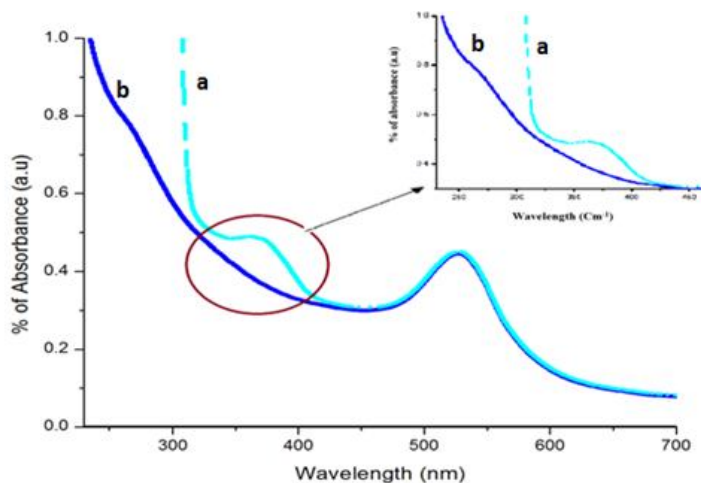
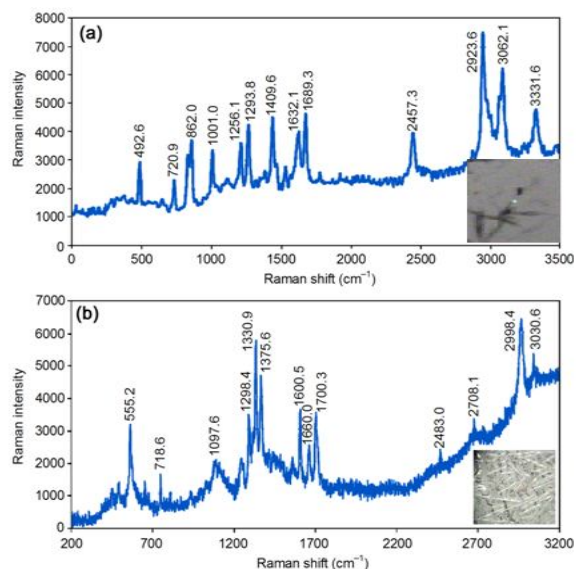


**Figure 3.1.** UV-vis absorption spectra of a) caffeine and b) BTPPNTs-caffeine (**inset: Figure**).

### 3.2. CRM and CRS analysis

To explore the chemical participation of BTPPNTs and BTPPNTs-caffeine, CRS and CRM investigation has been performed (**Figures 3.2a** and **3.2b**). The Raman scattering of BTPPNTs-caffeine mainly shows the OH stretching and CH, NH bending frequencies as shown in **Table 3.1**. (3331 and 1097–1632  $\text{cm}^{-1}$ ), respectively [33–35, 38]. In addition to that 1689 and 3062  $\text{cm}^{-1}$  indicates the presence of carbonyl and NH stretching vibrations as strong band. The CRM result further indicated active surface morphology of BTPPNTs-caffeine (**inset: Figure**), which will be ideal for the surface enhanced vibrational activity [39–42].

**Figure 3.2.** Confocal Raman microscopic spectra of a) BTPPNTs and b) BTPPNTs-caffeine (**inset shows BTPPNTs and BTPPNTs-caffeine CRM image**).



The CRM vibrational assignments are compared in **Table 3.1**. The CRM images are equivalent to the HR-SEM and HR-TEM micrographs, which are briefly described.

**Table 3.1. Experimental CRS, FT-Raman and computed Raman vibrational frequencies of BTTPNTs, caffeine and BTTPNTs-caffeine with their assignments.**

FT-Raman frequencies (cm <sup>-1</sup> )			Computed Raman frequencies (cm <sup>-1</sup> )			Confocal Raman frequencies (cm <sup>-1</sup> )		Assignments*
BTTPNTs	Caffeine [24]	BTTPNTs-caffeine	BTTPNTs	Caffeine	BTTPNTs-caffeine	BTTPNTs	BTTPNTs-caffeine	
363.6w	390.3w	-	386.2	354.1	363.4	-	-	$\pi$ CH <sub>2</sub> bending (C <sub>8</sub> )
410.7w	442.7m	408.0s	402.7	-	413.0	-	-	$\mu$ C-N bending (C <sub>19</sub> )
-	484.4m	-	-	-	482.2	492.6m	-	$\pi$ N-C bending (C <sub>22</sub> )
-	556.2s	-	-	551.1	549.3	-	555.2s	$\omega$ CH <sub>2</sub> bending (C <sub>14</sub> )
620.8m	644.6m	-	606.3	-	-	-	-	$\rho$ C-F in-plane bending (C <sub>35</sub> )
760.6m	741.3m	796.2w	720.1	747.4	719.8	720.9w	718.6w	$\omega$ C-NH in-plane bending (C <sub>10</sub> )
827.5s	928.7w	-	830.4	810.0	-	862.0m	-	$\omega$ CH <sub>2</sub> bending (C <sub>11</sub> )
1001.7s	1073.1m	1084.6s	1098.2	1054.6	1083.1	1001.0m	1097.6s	$\rho$ C-H out-of-plane bending (C <sub>37</sub> )
1153.3m	-	1187.4s	1160.0	1118.8	1092.5	-	-	$\omega$ CH bending (C <sub>7</sub> )
1207.4m	1241.8m	1248.6s	1214.7	1228.6	1250.4	1256.1m	1298.4m	$\pi$ CH <sub>3</sub> bending (C <sub>33-35</sub> )
1298.9m	1255.0m	1253.2m	-	1290.1	1299.0	1293.8s	1310.9w	$\mu$ C-O-N bending (C <sub>30</sub> )
1335.5s	1360.2m	1376.9m	1320.9	1340.5	1375.9	-	1381.3s	$\nu$ CH <sub>2</sub> sym. (C <sub>8</sub> )
1441.2m	1408.2m	-	1353.2	-	1437.2	1409.6s	-	$\omega$ CH ring bending
-	1470.0w	-	-	1460.5	1460.2	-	-	$\omega$ CH+CH <sub>3</sub> bending (C <sub>9</sub> )
1584.5s	1554.2m	1569.3m	1560.1	1543.2	1571.5	-	-	$\rho$ NH+pyrimidine ring
1605.0m	1600.8w	-	1635.0	1607.9	1637.6	1632.1m	1600.5w	$\pi$ CH <sub>3</sub> bending (C <sub>35</sub> )
1688.4w	1654.4w	1680.0s	1701.9	1691.1	1680.1	1689.3s	1660.0m	$\nu$ C-O-N stretching (O <sub>27</sub> )
1721.8m	1698.6m	1709.8s	1730.2	1772.6	1731.3	-	1700.3w	$\nu$ C=O sym. (O <sub>12</sub> )
-	-	1846.1s	1860.0	1841.8	1836.0	-	-	$\nu$ C=O sym. (O <sub>34</sub> )
-	2142.0w	2148.5m	2160.3	-	2066.0	-	-	$\rho$ O-N-H in-plane bending (N <sub>2</sub> )
-	-	2482.0s	2316.7	-	2077.4	-	-	$\nu$ N-CH sym. (C <sub>10</sub> )
2588.3w	-	2582.9w	2580.0	-	-	2457.3m	2483.0w	$\nu$ C=C sym. (ring)
2874.1m	-	2618.5m	2872.2	-	3029.9	-	2708.1w	$\nu$ CH <sub>2</sub> asym. (C <sub>8</sub> )
2934.9s	2957.6s	2987.2s	2903.8	-	3094.6	2923.6s	2998.4s	$\nu$ CH+CH <sub>3</sub> asym. (C <sub>4</sub> )
3006.7w	3113.1m	3150.4m	3126.4	3194.8	3118.8	3062.1s	-	$\nu$ N-H sym. (N <sub>30</sub> )
3059.6s	-	3270.0m	3387.9	-	3363.6	3331.6m	3030.6s	$\nu$ CH sym. (C <sub>7</sub> )

v – stretching;  $\rho$  – rocking;  $\omega$  – wagging;  $\pi$  – scissoring;  $\mu$  – twisting; w – weak; m – medium; s – strong.

\*From the references of [27], [32] and [36–42].

### 3.3. FT-Raman spectral analysis of BTTPNTs and BTTPNTs-caffeine

Experimental and computed FT-Raman spectra of BTTPNTs and BTTPNTs-caffeine are displayed in **Figures 3.3** and **3.4**. Observed Raman frequencies are compared in **Table 3.1** along with their assignment based on the literatures [27,32,36–43]. **Figures 3.3a** and **3.4a** display the spectra of BTTPNTs in region of 1600–400 cm<sup>-1</sup>. The weak band at 363 cm<sup>-1</sup> has been assigned to CH<sub>2</sub> bending

vibrations, whereas a strong band at  $1335\text{ cm}^{-1}$  is attributed to the  $\text{CH}_2$  stretching vibrations, and  $1180\text{ cm}^{-1}$  has been assigned to Tryptophan bending vibration. Raman frequency at  $620\text{ cm}^{-1}$  is assigned to C–F bending vibration. Bands at  $760$  and  $1084\text{ cm}^{-1}$  are due to N–H and CH bending vibrations, respectively. A band appeared at  $1441\text{ cm}^{-1}$  is assigned to CH ring bending vibration and  $1207\text{ cm}^{-1}$  band is attributed to  $\text{CH}_3$  bending vibrations, respectively. Caffeine spectral data displays the range at  $1700\text{--}400\text{ cm}^{-1}$ . A weak absorption band to medium signals corresponding to C–C bending, CH, NH stretching and bending of pyrimidine ring vibrations, respectively. The higher frequency ranges at  $2142$ ,  $2957$  and  $3113\text{ cm}^{-1}$  represents to O–NH in-plane bending, CH,  $\text{CH}_3$  asymmetric and NH symmetric stretching vibrations (listed as **Table 3.1**). **Figures 3.3b** and **3.4b** the observed frequencies of Raman spectrum of BTPPNTs-caffeine is compared with the observed frequencies of BTPPNTs and caffeine. The carbonyl group is expected to appearing in the range of  $1680$  to  $1850\text{ cm}^{-1}$  present in all the three systems *viz.*, BTPPNTs, caffeine and BTPPNTs-caffeine it often indicates the charge transfer from caffeine to BTPPNTs [17,44]. The  $\text{CH}_2$  and C–O–N bending vibration which are appeared at  $827$  and  $1253\text{ cm}^{-1}$  are enhanced due to the charge transfer between  $\pi$  electron-rich –CO– moiety of the caffeine and BTPPNTs. This shift may be taken as the evidence of caffeine-amino group interaction. The strong band at  $1084\text{ cm}^{-1}$  is assigned to C–N bending vibration showed a blue shift from  $410\text{ cm}^{-1}$  in the FT-Raman spectrum of BTPPNTs, which also evinced the electron donation from the nitrogen atom to the caffeine molecules. The large magnitude of the red shift of this band observed at  $3270\text{ cm}^{-1}$  is confirmed caffeine interaction with BTPPNTs. From these observation it can be concluded that, caffeine is chemisorbed to the surface of BTPPNTs. SERS has the capability, making BTPPNTs-caffeine is showing SERS activity and it creates sensitivity. The experimental vibrational assignments were compared with computed Raman frequencies. The adsorption motivates that further design of BTPPNTs-caffeine for applications like drug delivery system (DDS) and designing biosensors.

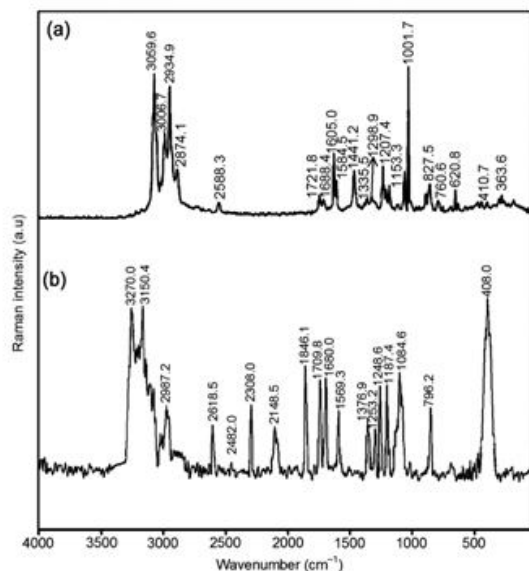


**Figure 3.3.** Experimental FT-Raman spectra of a) BTPPNTs and b) BTPPNTs-caffeine.

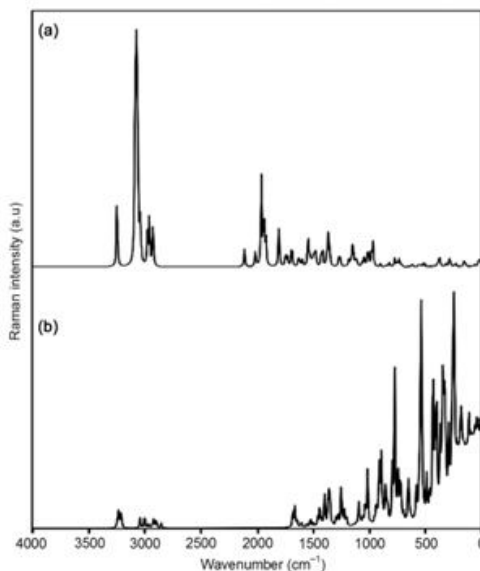


**Figure 3.4.** Computed Raman spectra of a) BTPPNTs and b) BTPPNTs-caffeine.

### 3.4. HR-TEM analysis

The morphology of the resulted BTPPNTs-caffeine is predicted by HR-TEM micrograph analysis. **Figure 3.5** represents the HR-TEM micrographs of the as-synthesized BTPPNTs-caffeine at different

magnifications. The synthesized BTPNTs-caffeine showing a well-defined tubular shaped and nanovesicles with dense pore with implanted-caffeine. The sizes of nanotubes are having 23.6 to 19.2 nm range is defined by image J program. **Figures 3.5a–3.5d** clearly revealed the BTPNTs-caffeine is having tubular like structure. The lattice fringe orientation in the HR-TEM image also confirms this observation (**Figure. 3.5d**) [37].

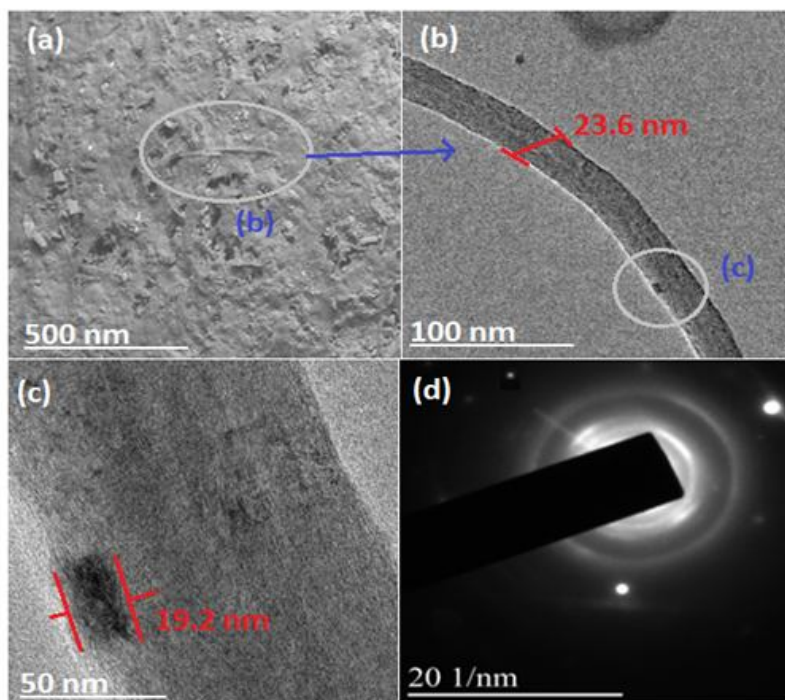


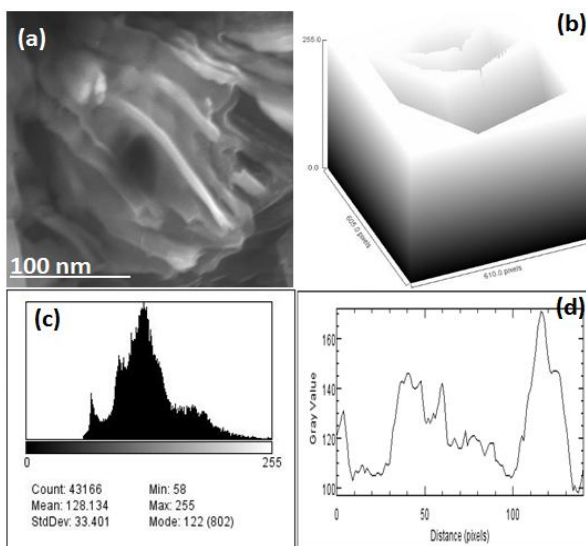
**Figure 3.5.** HR-TEM micrographs of BTPNTs-caffeine at different magnifications of a) 500 nm, b) 100 nm, c) 50 nm and d) SAED pattern.

### 3.5. HR-SEM analysis

HR-SEM image of BTPNTs-caffeine (**Figures 3.6a–3.6d**) is very similar to the HR-TEM and CRM image shown in **Figure 3.2**. The HR-SEM image exposed the surface morphology of various nanosized (~23 nm) and mixed a nanotube and nanovesicles (**Figure 3.6a**). The HR-SEM images of the BTPNTs-caffeine shows and two different surface mappings in highlighted in **Figures. 3.6b** and **3.6c** [32,44]. The average particle size range of ~21 nm and the particle distribution plot and total surface area plots were simulated with image J program (**Figure 3.6d**).

**Figure. 3.6.** a) HR-SEM image of BTPNTs-caffeine, b) highlighted particle distribution surface plot, c) particle distribution plot profile and d) total surface plot profile.

### 3.6. Optimized molecular geometry



The optimized structural parameters like bond lengths between various atoms of BTPNTs-caffeine shown in the **Figure 3.7**. The theoretical model shows comparable structural parameters with the observed literature values [45]. The optimized molecular geometrical parameters of BTPNTs-caffeine clearly shows some important typical bond lengths between the respective atoms *viz.*,  $\sigma$ -C1(sp<sup>2</sup>)-C6(sp<sup>2</sup>) and C15(sp<sup>2</sup>)-C20(sp<sup>2</sup>) of BTPNTs moiety = 0.82 Å,  $\sigma$ -C22(sp<sup>2</sup>)-C33(sp<sup>2</sup>) of caffeine ring = 0.77 Å,  $\sigma$ -N23(sp<sup>3</sup>)-C24(sp<sup>2</sup>) = 0.82 Å,  $\sigma$ (C-O) = 0.78 Å,  $\sigma$ (O-H) = 0.82 Å,  $\sigma$ (N-H) = 0.83 Å and  $\sigma$ (C-F) = 0.82 Å. The existences of H-bonding and other electronic effects *viz.*, Van der Waals interactions or proton transfer phenomena if any, are ceases to exist in the gaseous phase of molecules, it's responsible for the formation of BTPNTs.

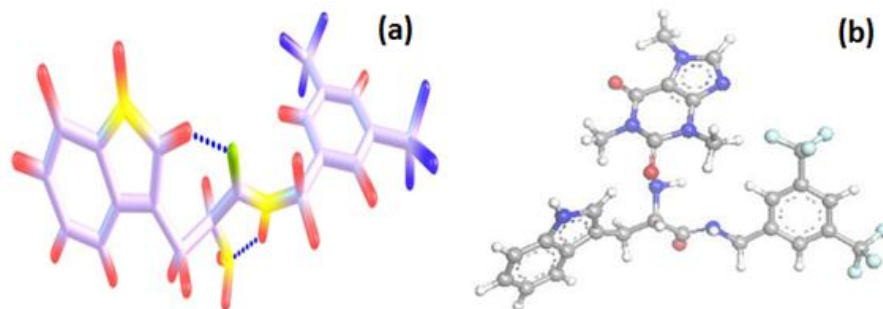


**Figure. 3.7. Optimized geometries of a) BTPNTs and b) BTPNTs-caffeine.**

### 3.7. Frontier molecular orbital analysis

In caffeine and BTPNTs-caffeine there are 51 and 317 valence electrons constituting the molecular orbitals in which the highest occupied molecular orbital (HOMO) with anti-symmetric properties (A) having energy of about -0.24 and -0.27 amu and the lowest unoccupied molecular orbital (LUMO) with energy of about -0.05 and -0.17 amu. Among 51 and 161 molecular orbitals, those atomic orbital's which are all mainly contributing towards the HOMO-LUMO can be easily visualized from the **Figures 3.8a** and **3.8b**. Evidently, the HOMO as well as LUMO of caffeine and BTPNTs-caffeine is primarily a linear combination of atomic orbitals of nitrogen and the caffeine [12, 46]. The energy gap or excitation energy between those frontier molecular orbital is determined and found to be  $\Delta E_{\text{LUMO-HOMO}} = 0.19$  and  $0.10$  amu.  $\Delta E = E_{\text{LUMO}} - E_{\text{HOMO}}$  is calculated  $[-0.05 - (-0.24)]$  and  $[-0.17 - (-0.27)]$  amu and found to be as  $0.19$  and  $0.10$  amu (or)  $1.02$  and  $2.12$  kcal mol<sup>-1</sup>, respectively.

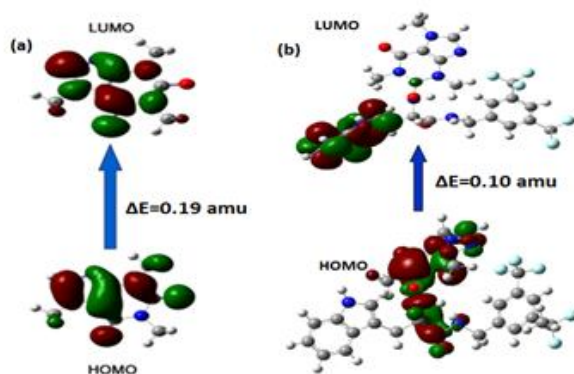


**Figure 3.8. HOMO-LUMO diagrams of a) caffeine and b) BTPNTs-caffeine.**

### 3.8. Density of state (DOS) analysis

Theoretical investigations done on BTPPNTs (Figure 3.9a) and BTPPNTs-caffeine (Figure 3.9b). The electron density of states (DOS) caffeine covalently interacted with BTPPNTs presents two characteristic peaks, both extending 3.02 and 2.12 eV below and above the energy gap, respectively. Both correspond to states having p character, mainly spread over the H<sub>2</sub>N-caffeine site of the self-assembly [37, 46]. This aspect reveals that an interaction through the binding site of the caffeine is not altering the structure but to induce the activity like SERS and sensing.

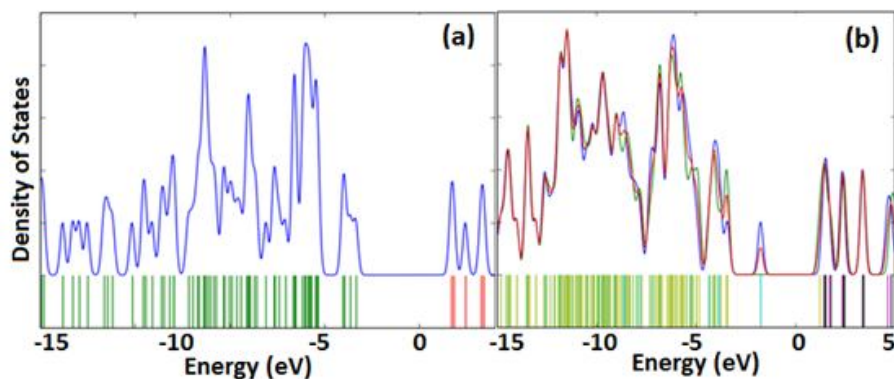


Figure 3.9. DOS plots of a) BTPPNTs and b) BTPPNTs-caffeine {BTPPNTs (green), caffeine (red) and BTPPNTs-caffeine (blue)}.

## 4. CONCLUSION

BTPPNTs-caffeine was characterized by a choice of spectral and microscopic techniques. The UV-vis spectral results indicate the formation of BTPPNTs interacted with caffeine *viz.*, mainly through CO and NH<sub>2</sub> groups. The microscopic results were predicted to the formation of peptide nanotubes and its size is roughly 21 nm. FT-Raman results showed the information about the BTPPNTs for employing SERS and sensing probe has been achieved by using caffeine medium. The sensing ability is supported for the help of DOS studies; it gives the trace detection of biological processes like drug delivery applications (DDS). DOS plot and UV-vis results provide the information about the bond energy decreases, it increases the active sites and identification mechanism of cells via, *in-situ* applications through solvent medium. Combining the SERS, DOS plots predicts the positive information about the carrying and sensing abilities of the BTPPNTs.

## ACKNOWLEDGEMENT

The authors thank to A.K. Giri and Prof. V.J. Hruby Department of Chemistry and Biochemistry, University of Arizona, USA, for the help in the synthesis of peptide. The authors are grateful to FEAT, Annamalai University to providing HR-SEM facility. HR-TEM images were recorded at Centre for Nanoscience and Nanotechnology, Sathyabama University, Chennai.

## CONFLICT OF INTEREST

The authors declare no competing financial interest.

## REFERENCES

- [1] H.G.M. Edwards, T. Munshi, M. Anstis, *Spectrochim. Acta A*, 61 (2005) 1453–1459.
- [2] N.O. Johnson, T.P. Light, G. McDonald, Y. Zhang, *J. Phys. Chem. B* 121 (2017) 1649–1659.
- [3] M. Shi, L.Y. Huang, N. Nie, J.H. Ye, X.Q. Zheng, J.L. Lu, Y.R. Liang, *Food Res. Int.* 93 (2017) 1–7.
- [4] N. Abhari, A. Madadlou, A. Dini, O. Hosseini Naveh, *Food Chem.* 214 (2017) 16–24.
- [5] W. Wang, S. Ye, *Phys.Chem.Chem.Phys.* 19 (2017) 4488–4493.

- [6] C.S. Perry III, A.K. Thomas, H.A. Taylor, P.F. Jacques, R.B. Kanarek, *Appetite* 107 (2016) 69–78.
- [7] R. Kamalakannan, G. Mani, P. Muthusamy, A. Susaimanickam, K. Kim, *J. Indust. Eng. Chem.* 51 (2017) 113–121.
- [8] L. Tavagnacco, J.W. Brady, A. Cesaro, *Food Biophys.* 8 (2013) 216–222.
- [9] M.O. Okuom, M.V. Wilson, A. Jackson, A.E. Holmes, *Int. J. Spectrosc.* 2013 (2013) 1–6.
- [10] M. Ajit Kumar, P. Sahoo, S. Goswami, H.K. Fun, C.S. Yeap, *J. Inclu. Phenom. Macrocycl. Chem.* 67 (2010) 99–108.
- [11] C. Siering, B. Beermann, S.R. Waldvogel, *Supramol. Chem.* 18 (2006) 23–27.
- [12] Y. Song, S.R. Challa, C.J. Medforth, Y. Qiu, R.K. Watt, D. Pen, J.E. Miller, F.V. Swol, J.A. Shelnutt, *Chem. Commun.* (2004) 1044–1045.
- [13] S. Ray, M.G.B. Drew, A.K. Das, A. Banerjee, *Tetrahedron Lett.* 62 (2006) 7274–7283.
- [14] M.T. Crimmins, P.J. McDougall, *Org. Lett.* 5 (2003) 591–601.
- [15] S. Gilead, E. Gazit, *Supramol. Chem.* 17 (2005) 87–92.
- [16] S. Parween, A. Misra, *J. Mater. Chem. B* 2 (2014) 3096–3106.
- [17] M.L. Waters, *J. Biopolymers* 76 (2004) 435–445.
- [18] J.S. Davies, *J. Pept. Sci.* 9 (2003) 471–501.
- [19] S. Fleming, R.V. Ulijn, *Chem. Soc. Rev.* 43 (2014) 8150–8177.
- [20] D.W. Su, Y.C. Wang, *Tetrahedron Lett.* 40 (1999) 4197–4207.
- [21] Y. Verdier, M. Zarandi, *J. Pept. Sci.* 10 (2004) 229–248.
- [22] B. Karthikeyan, A.K. Giri, *J. Microsc. Ultrastruct.* 2 (2014) 224–229.
- [23] I. Azuri, L.A. Abramovich, *J. Am. Chem. Soc.* 136 (2014) 963–969.
- [24] M. Manivannan, K. Rajeshwaran, R. Govindhan, B. Karthikeyan, *J. Mol. Struct.* 1144 (2017) 432–442.
- [25] S. Marchesan, A.V. Vargiu, *Molecules*, 20 (2015) 19775–19788.
- [26] B. Karthikeyan and R. Govindhan, *Sens. Lett.*, 16 (2018) 1–8.
- [27] T. Pradeep, *Nano the essential*, Tata McGraw Hill Edu. Pvt. Ltd., 2007, p. 275.
- [28] B. Karthikeyan, A.K. Giri, V.J. Hruby, *J. Sol-Gel Sci. Technol.* 72 (2014) 534–542.
- [29] J.A. Leiro, M. Torhola and K. Laajalehto, *J. Phys. Chem. Solids* 100 (2017) 40–44.
- [30] L.A. Abramovich, M. Raches, *New J. Chem.* 28 (2004) 14021–1411.
- [31] J.H. Collier, T. Segura, *J. Biomater.* 32 (2011) 4198–4204.
- [32] K. Reena, M. Gajendiran, M. Prabakaran, S. Arul Antony, K. Kyobum, *J. Indust. Eng. Chem.* 51 (2017) 113–121.
- [33] T.A. Saleh, A. Sari, M. Tuzen, *J. Mol. Liq.* 219 (2016) 937–945.
- [34] D. O'Hagan, C. Schaffrath, *Nature* (London) 416 (2002) 279–286.
- [35] Z. Liu, M. Winters, M. Holodniy, H. Dai, *Angew. Chem. Int. Ed. Engl.* 46 (2007) 2023–2027.
- [36] A. Negar, M. Ashkan, D. Ali, H.N. Ozra, *Food Chem.* 214 (2017) 16–24.
- [37] R. Govindhan and B. Karthikeyan, *Data Brief*, 14 (2017) 579–583.
- [38] R. Govindhan and B. Karthikeyan, *J. Phys. Chem. Solids*, 111 (2017) 123–134.
- [39] M.J. Frisch, G.W. Trucks, H.B. Schlegel, G.E. Scuseria, M.A. Robb, J.R. Cheeseman, G. Scalmani, V. Barone, B. Mennucci, G.A. Petersson, H. Nakatsuji, M. Caricato, X. Li, H.P. Hratchian, A.F. Izmaylov, J. Bloino, G. Zheng, J.L. Sonnenberg, M. Hada, M. Ehara, K. Toyota, R. Fukuda, J. Hasegawa, M. Ishida, T. Nakajima, Y. Honda, O. Kitao, H. Nakai, T. Vreven, J.A. Montgomery Jr, J.E. Peralta, F. Ogliaro, M. Bearpark, J.J. Heyd, E. Brothers, K.N. Kudin, V.N. Staroverov, T. Keith, R. Kobayashi, J. Normand, K. Raghavachari, A. Rendell, J.C. Burant, S.S. Iyengar, J. Tomasi, M. Cossi, N. Rega, J.M. Millam, M. Klene, J.E. Knox, J.B. Cross, V. Bakken, C. Adamo, J. Jaramillo, R. Gomperts, R.E. Stratmann, O. Yazyev, A.J. Austin, R. Cammi, C. Pomelli, J.W. Ochterski, R.L. Martin, K. Morokuma, V.G. Zakrzewski, G.A. Voth, P. Salvador, J.J. Dannenberg, S. Dapprich, A.D. Daniels, O. Farkas, J.B. Foresman, J.V. Ortiz, J. Cioslowski, D.J. Fox, Gaussian, Inc., Wallingford CT, *Gaussian 09*, Revision C.01, 2010.
- [40] N.M. O'Boyle, A.L. Tenderholt, K.M. Langner, *J. Comp. Chem.* 29 (2008) 839–845.
- [41] L. Jinghui, K.T.S. Sebastian, A.G. Warmlander, A. Jan Pieter, *J. Biol. Chem.* 291 (2016) 16485–16493.
- [42] R. Govindhan and B. Karthikeyan, *J. Mol. Struct.*, 1156 (2018) 51–61.

- 
- [43]A. Saleh, M.M. Al-Shalalfeh, T.A. Onawole, A.A. Al-Saadi, *Vib. Spectrosc.* 90 (2017) 96–103.  
[44]S.V. Paston, A.M. Polyanichko, O.V. Shulenina, *J. Struct. Chem.* 58 (2017) 399–405.  
[45]R. Govindhan and B. Karthikeyan, *J. Adv. Microsc. Res.*13 (2018) 1–7.  
[46]B. Karthikeyan, M. Murugavelu, *Sens. Actuators B* 163 (2012) 216–223.